Passive Cooling of a Granular Medium inside a Cylindrical Chamber

Vitor J. Petry[1], Alvaro L. De Bortoli[1], Oleg Khatchatourian[2]

[1] UFRGS-IM/DMPA/PPGMAp - Graduate Program in Applied Mathematics
Av. Bento Gonçalves, 9500 - P. O. Box 15080, Porto Alegre, RS - Brazil
Email: vpetry@mat.ufrgs.br, dbortoli@mat.ufrgs.br
[2] UNIJUI - Department of Physics, Statistics and Mathematics,
R. São Francisco 501, P.O. Box 560, Ijui - RS
olegkha@admijui.unijui.tche.br

Abstract. In several engineering and applied mathematics situations we are interested to evaluate the heat and mass transfer in granular media. In this work we are interested to evaluate the passive cooling of heat generating spheres inside a cylindrical chamber. Some numerical tests are realized to evaluate the parameters influence such as the chamber radius, the spheres humidity and the chamber material. The mathematical model can be applied to small load nuclear reactors safety where the spheres are fuel elements. It can also be applied to the grains drying process, where the air flow needs to be included.

1 Introduction

In this work we introduce a mathematical model to calculate the heat and mass transfer in granular medium (small spheres) inside a cylindrical chamber. We consider that the spheres generate heat and they are surrounded by air. There is heat and mass transfer from spheres to the air, since in the beginning the spheres are humid.

The governing equations are numerically resolved using first time and second order space approximations, based on the finite difference approach; numerical stability and convergence conditions are also analyzed. Moreover, we present some simulations showing the influence of certain parameter variations in the mass and heat transfer process. The thermal balance is realized for the spheres and the air which involve them. The heat transfer is given by the conduction process inside the chamber and through the walls. On the external surface, the heat change with the atmosphere is given by the convection and the radiation processes.

As the main applications of the model, we highlighted the safety of a small load nuclear reactor in the case of an accident [4] and in the grains drying processes.

2 Governing Equations and Solution Procedure

The fixed bed chamber consists of one cylindrical tube inside which spheres of $15mm$ diameter are deposited (in the reactor case), as shown in Fig. 1. We consider that the spheres inside the chamber generate heat and contain a certain initial humidity [4]. The mathematical model here adopted consider the set of governing equations to describe the temperature distribution inside the chamber and the humidity in the air and inside the spheres. The following hypothesis were adopted:

- the medium porosity is constant;
- there is thermal equilibrium between the spheres and the air inside the chamber;
- there is mass transference from the spheres to the air;
- the heat transfer occurs at radial direction;
- the chamber walls are made of steel;
- the transference of heat through the walls is by conduction;
- the heat transference to the air occurs by radiation and convection, neglecting the conduction.

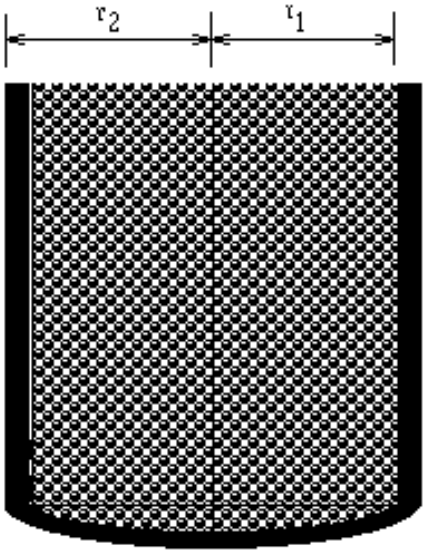

Fig. 1. Sketch of the chamber

2.1 Governing equations

The set of governing equations include the mass conservation, for air and solid, and energy, to the walls and inside the chamber.

Mass conservation for air: The mass equation comes from the balance inside the control volume [1]. It results for the air humidity Y:

$$\frac{\partial Y}{\partial t} = \frac{D}{r}\frac{\partial}{\partial r}\left(r\frac{\partial Y}{\partial r}\right) + \dot{m} \tag{1}$$

From mass conservation, the water mass, which goes to the air, is equal to that which leaves the spheres [3]. Therefore, it results for the mass generation rate:

$$\dot{m} = -\frac{1}{\phi V_c}\frac{\partial m_l}{\partial t} \tag{2}$$

or

$$\dot{m} = aD_{sg}\frac{(1-\phi)}{\phi}\Delta C \tag{3}$$

where a is the sphere area to volume ratio, ϕ the bed porosity, V_c the control volume and $\Delta C = (\rho_s X - \rho_g Y)$ the mass concentration variation, with X the ratio of spheres humidity.

The values of mass diffusion coefficients D and D_{sg} were set as constants when writing the equations; however, they are recalculated when performing the iterations.

Mass conservation for solid: From equations (2) and (3) it follows that:

$$\frac{\partial m_l}{\partial t} = -V_c a D_{sg}\left(1-\phi\right)\Delta C \tag{4}$$

as a consequence we have:

$$\frac{\partial X}{\partial t} = -\frac{aD_{sg}\left(\rho_s X - \rho_g Y\right)}{\rho_s} \tag{5}$$

where the subscripts s, l and g represent the solid, liquid and gas (air), respectively.

Energy equation inside the chamber: The energy equation in cylindrical coordinates, for the chamber in thermal equilibrium, results:

$$\left(\rho c_p\right)^* \frac{\partial T}{\partial t} = \frac{k^*}{r}\frac{\partial}{\partial r}\left(r\frac{\partial T}{\partial r}\right) + \dot{q_1} - \dot{q_2} \tag{6}$$

where $\dot{q_1}$ and $\dot{q_2}$ are the rates of heat generation by the fuel elements and the energy consumed by water evaporation which leaves the spheres by unit of time and volume, respectively, which are given by:

$$\dot{q_1} = 0.095 q_o t^{-\beta} \tag{7}$$

and:

$$\dot{q_2} = \dot{m} H_v = \frac{a D_{sg} (1-\phi) \Delta C}{\phi} H_v \tag{8}$$

where q_o is the initial heat generation rate and H_v the water evaporation latent heat. Defining α^* and $(\rho c_p)^*$ as the thermal diffusivity and the product of the density and specific heat at constant pressure of the mass inside the chamber, respectively, it follows that:

$$\alpha^* = (1-\phi)\,\alpha_s + \phi \alpha_g \tag{9}$$

$$(\rho c_p)^* = (1-\phi)\,\rho_s c_{p_s} + \phi \rho_g c_{p_g} \tag{10}$$

As the thermal conductivity values vary with the temperature, they are calculated using the following expressions:

$$\alpha_g (T) = 2 \times 10^{-9} T^{1.655} \tag{11}$$

$$\rho_g c_{p_g} (T) = 172645 T^{-0.8795} \tag{12}$$

$$\rho_g (T) = 349.01 T^{-1.0003} \tag{13}$$

Energy equation for the walls: For the walls the energy equation can be written as follows:

$$\frac{\partial T}{\partial t} = \frac{\alpha_w}{r} \frac{\partial T}{\partial r} + \alpha_w \frac{\partial^2 T}{\partial r^2} \tag{14}$$

where α_w is the walls thermal conductivity.

2.2 Boundary and initial conditions

The appropriate implementation of boundary conditions is always important when solving a set of differential equations. Here some assumptions are adopted as following indicated.

Initial and boundary conditions inside the chamber: When starting the simulations, the temperature, the air and the spheres humidity are considered constant. So, at time $t = 0$, it results:

$$X(0,r) = X_i, \qquad Y(0,r) = Y_i \qquad T(0,r) = T_{c_i} \tag{15}$$

For $r = 0$ and $r = r_1$, results for the Neumann conditions:

$$\frac{\partial Y}{\partial r}(t,0) = \frac{\partial X}{\partial r}(t,0) = \frac{\partial T}{\partial r}(t,0) = 0 \qquad \frac{\partial Y}{\partial r}(t,r_1) = \frac{\partial X}{\partial r}(t,r_1) = 0 \quad (16)$$

The temperature at $r = r_1$ is equal to the wall temperature.

Initial and boundary conditions for the chamber walls: At time $t = 0$ the temperature is equal to the ambient temperature, outside the chamber.

$$T(0,r) = T_{amb} \quad (17)$$

At external surface ($r = r_2$) the heat transference occurs by radiation and by natural convection. Therefore, the boundary condition results:

$$-k_w \frac{\partial T}{\partial r}(t,r_2) = \dot{q_{rad}} + \dot{q_{con}} \quad (18)$$

where

$$\dot{q_{rad}} = \gamma\sigma\left(T^4(r_2) - T_{amb}^4\right) \quad (19)$$

$$\dot{q_{con}} = 2.13\left(T(r_2) - T_{amb}\right)^{1.31} \quad (20)$$

2.3 Finite difference approximation and corresponding numerical analysis

The finite difference Gauss-Seidel approach is employed to obtain the numerical results. First order time and a second order space approximations are used, as follows:

$$\frac{\partial \Psi}{\partial t} \approx \frac{\Psi_j^{n+1} - \Psi_j^n}{\Delta t} \quad (21)$$

$$\frac{\partial \Psi}{\partial r} \approx \frac{\Psi_{j+1}^n - \Psi_{j-1}^n}{2\Delta r} \quad (22)$$

$$\frac{\partial^2 \Psi}{\partial r^2} \approx \frac{\Psi_{j+1}^n - 2\Psi_j^n + \Psi_{j-1}^n}{(\Delta r)^2} \quad (23)$$

Equations (1), (6) and (14) can be writen in the following way:

$$\frac{\partial \Psi}{\partial t} = \lambda\left[\frac{1}{r}\frac{\partial \Psi}{\partial r} + \frac{\partial^2 \Psi}{\partial r^2}\right] + F \quad (24)$$

Considering the homogeneous case (for $F = 0$) and using the approximations (21-23), we have:

$$\Psi_j^{n+1} = \frac{\lambda \Delta t}{2j\left(\Delta r\right)^2}\left[\Psi_{j+1}^n - \Psi_{j-1}^n\right] + \frac{\lambda \Delta t}{\left(\Delta r\right)^2}\left[\Psi_{j+1}^n - 2\Psi_j^n + \Psi_{j-1}^n\right] + \Psi_j^n \tag{25}$$

where $r = j\Delta r$. Denoting $y = \frac{\lambda \Delta t}{(\Delta r)^2}$ we have:

$$\Psi_j^{n+1} = \left[\frac{y}{2j} + y\right]\Psi_{j+1}^n + \left[1 - 2y\right]\Psi_j^n + \left[y - \frac{y}{2j}\right]\Psi_{j-1}^n \tag{26}$$

Applying the discret Fourier transform, the equation (26) results in:

$$\overline{\Psi^{n+1}} = \left[\left(\frac{y}{2j} + y\right)e^{ix} + 1 - 2y + \left(y - \frac{y}{2j}\right)e^{-ix}\right]\overline{\Psi^n} \tag{27}$$

Thus, the Fourier symbol is given by:

$$S\left(x\right) = 1 - 2y\left(1 - \cos(x)\right) + i\frac{y}{j}\sin(x) \tag{28}$$

The scheme is stable if and only if $\left|S\left(x\right)\right| \leq 1$, for all , $x \in [-\pi, \pi]$ that is if and only if:

$$\frac{y^2}{j^2}\sin^2\left(x\right) + 4y^2\left(1 - \cos\left(x\right)\right)^2 - 4y\left(1 - \cos\left(x\right)\right) \leq 0 \tag{29}$$

Fig. 2 shows that for $j = 1$ the scheme is stable if $y \leq \frac{1}{2}$; for $y > \frac{1}{2}$ we observe that the scheme is not stable. The same results are observed for $j > 1$. For $j = 0$ we adopted the boundary condition $\frac{\partial \Psi}{\partial r} = 0$, what implies that $\Psi_{j-1}^n = \Psi_{j+1}^n$ and we can write the equation (26) as follows:

$$\Psi_j^{n+1} = 2y\Psi_{j+1}^n + \left(1 - 2y\right)\Psi_j^n \tag{30}$$

Applying again the discreet Fourier transform, the Fourier symbol can be written as:

$$S\left(x\right) = 1 - 2y\left(1 - \cos(x)\right) + i2y\sin(x) \tag{31}$$

and again the stability condition of this scheme results in $y \leq \frac{1}{2}$.

Since the problem is well-posed and the scheme is consistent and stable for $y \leq \frac{1}{2}$, we have based on the Lax equivalence theorem [5] that the scheme is convergent.

3 Numerical Results

Numerical results are aimed to show the influence of certain parameters in the mass and heat transfer processes.

Except when the contrary is said, the physical characteristics of the chamber are [2]: $r_1 = 0.2m$, $r_2 = 0.22m$, $X_i = 0.005$, what corresponds approximately to 5% of water in volume, $Y_i = 0.0165$, what corresponds to air relative humidity

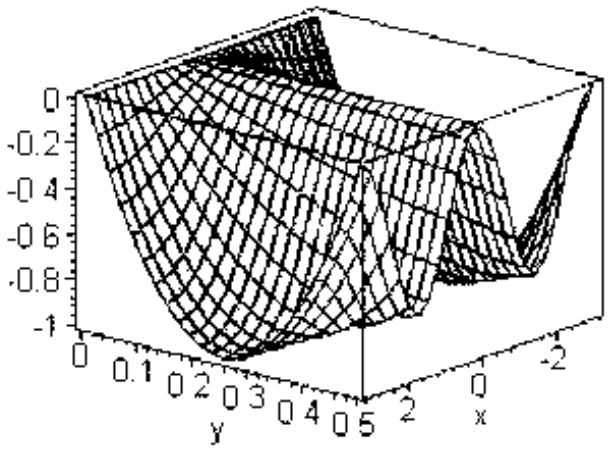

Fig. 2. Stability region

of order 60% and $\phi = 0.38$, $\sigma = 5.67 \times 10^{-8} Wm^{-2}K^{-4}$, $k_w = 15.1 Wm^{-1}K^{-1}$, $H_v = 2262600 Jkg^{-1}$, $\gamma = 0.2$, $\alpha_w = 3.91 \times 10^{-6} m^2 s^{-1}$, $q_o = 10^8 Wm^{-3}$, $\rho_s = 10500 kgm^{-3}$, $\alpha_s = 9.47 \times 10^{-7} m^2 s^{-1}$, $T_{c_i} = 590K$, $\beta = -0.26$, $T_{amb} = 298K$, $c_{p_s} = 402 Jkg^{-1}K^{-1}$, $\Delta t = 10^{-3} s$, $\Delta r = 10^{-3} m$.

The chamber walls material properties are that of AISI 302 steel. In the case of other material, other values need to by used.

Fig. 3 shows the temperature behavior at center and walls of the chamber; the temperature rises to its maximum value ($\approx 850K$ or $\approx 580°C$) during the first 45 minutes, when it starts to decrease. Such occurs because of the high heat generation when starting the process of passive cooling.

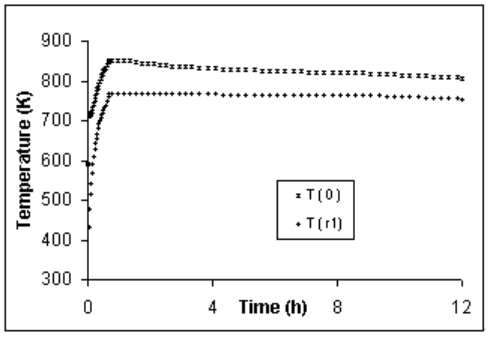

Fig. 3. Temperature of the chamber along the time for $r = 0$ and $r = r_1$

Fig. 4 presents the temperature distribution inside the chamber ($0 \leq r \leq r_1$). The temperature decreases from the chamber center to the walls; at tube walls the temperature remains almost constant, because metals are good conductors. The great time delay needed for chamber cooling happens due to the heat generation which decreases along the time.

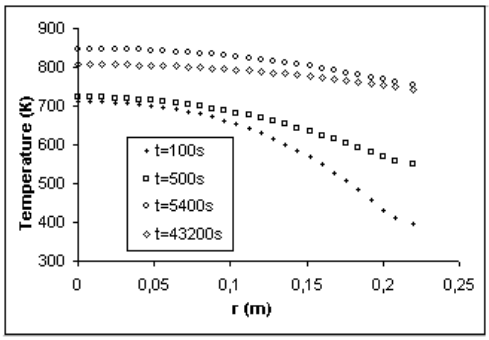

Fig. 4. Temperature distribution inside the chamber for $r = 0$ and $r = r_1$

Fig. 5 shows that the initial spheres humidity does not affect considerably the temperature distribution inside the chamber. The initial temperature fall on $r = r_1$ due to the walls which are cold.

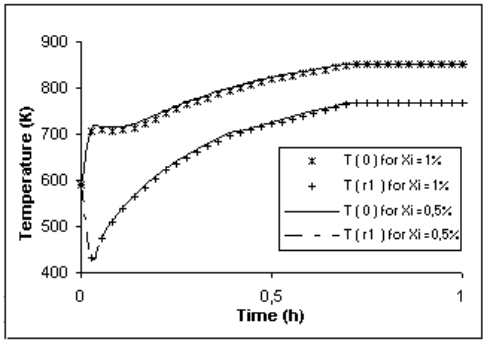

Fig. 5. Humidity influence on chamber temperature decrease

Fig. 6 shows the spheres humidity decrease along the time. Note that the initial humidity influences the moisture equilibrium between the solid and the air. This occurs because the humid air is not removed from the chamber. Since the

temperature in the chamber center is high, the air has large humidity absorption capacity; such justifies the large spheres humidity decrease in the chamber center.

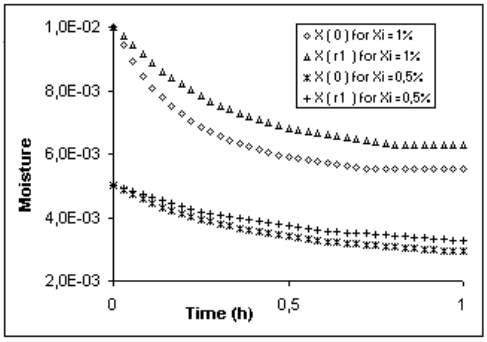

Fig. 6. Spheres humidity decrease along the time

The influence of the chamber walls material on the temperature distribution is analyzed considering two types of steel: the AISI 1010 and the AISI 302; that is illustrated in the Fig. 7. The properties of AISI 1010 steel are [2]: $k_w = 63.9 W m^{-1} K^{-1}$ and $\alpha_w = 1.88 \times 10^{-5} m^2 s^{-1}$. This result show that the material choose influences the temperature values and, consequently, other properties which are temperature dependent. While for the steel AISI 302 the temperature reaches to $850K$, with AISI 1010 its values arrives at $1130K$. On the other hand, Fig. 8 shows the influence of the chamber walls material on the air humidity distribution.

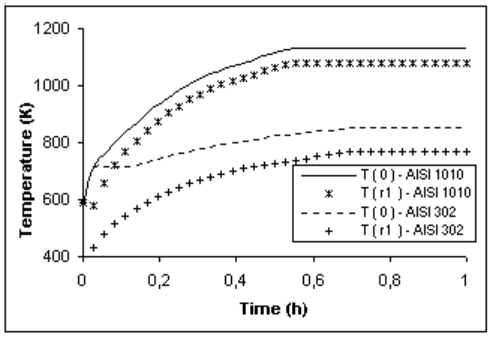

Fig. 7. Influence of the chamber walls material on the temperature distribution

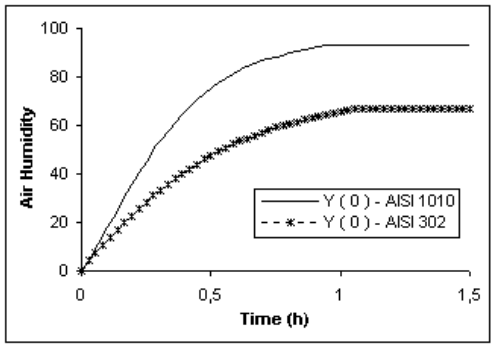

Fig. 8. Influence of the chamber walls material on the air humidity distribution

To verify the influence of the chamber dimensions on temperature, numerical simulations are realized for various chamber radius, maintaining the wall thickness (Fig. 9). When increasing the chamber diameter, the temperature rises significantly. That happens because there is more spheres, which generate more heat. Notice that while for $r_1 = 0.2m$ the temperature reaches around $850K$, for $r_1 = 0.3m$ its value increases to $990K$. In this way, for safety considerations of a reactor, it is advised to reduce the chamber diameter or to build another chamber type.

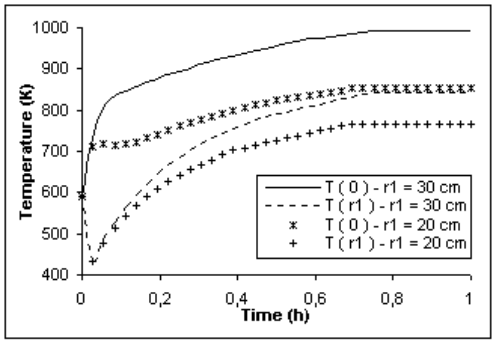

Fig. 9. Chamber dimensions influence on temperature increase

4 Conclusions

We have presented a mathematical model and a numerical scheme together with the stability and convergence conditions for the passive cooling of a granular medium inside a cylindrical chamber.

Obtained results indicate the importance of some parameters, dimensions and material type used for chamber walls. The smaller the chamber diameter, the better heat transfer is obtained. This analysis becomes important for the safety of nuclear reactors, for example. The model can also be used for the grains drying process, where the air flow needs to be introduced.

5 Acknowledgements

The work reported in this paper has been supported by CNPq (*Conselho Nacional de Desenvolviomento Científico e Tecnológico - Brasil*).

References

1. Bejan, A.: Advanced engineering thermodynamics, John Wiley Sons(1988).
2. Incropera, F. P.: Fundamentals of heat and mass transfer, John Wiley Sons (1990).
3. Khatchatourian, O., Borges, P. Petry, V., Weber, P.: A mathematical model for the drying process of soy grains in fixed bed, XXII CNMAC (1999).
4. Petry, V. J., De Bortoli, A. L., Sefidvash, F.: Passive cooling of a fixed bed nuclear reactor, Lavoisier (2005) 305–308.
5. Zeidler, E.: Nonlinear functional analysis and its applications, Springer-Verlag (1990).